HHS Public Access

Author manuscript

Nat Genet. Author manuscript; available in PMC 2017 October 10.

Published in final edited form as:

Nat Genet. 2017 May ; 49(5): 780–788. doi:10.1038/ng.3838.

Spatial heterogeneity in medulloblastoma

A full list of authors and affiliations appears at the end of the article.

Keywords

Spatial heterogeneity; medulloblastoma; glioblastoma multiforme; renal cell carcinoma; whole exome sequencing; gene expression profiling

Introductory paragraph

Spatial heterogeneity of transcriptional and genetic markers between physically isolated biopsies of a single patient's tumor poses major barriers to the identification of biomarkers, and the development of targeted therapies effective against the entire tumor. We analyzed spatial heterogeneity data from 35 patients with multi-regional biopsies using a combination of transcriptomic and genomic profiles. Medulloblastomas, but not malignant gliomas, demonstrate spatially homogeneous transcriptomes, allowing accurate subgrouping of tumors from a single biopsy. Conversely, somatic mutations that impact genes suitable for targeted therapeutics demonstrate high levels of spatial heterogeneity in medulloblastoma, malignant glioma, and renal cell carcinoma. Actionable targets found in a single medulloblastoma biopsy are seldom clonal across the entire tumor, questioning the efficacy

[#]Corresponding authors: Marco A. Marra, OBC, PhD, FRSC, FCAHS, Genome Sciences Centre. 675 West 10th Ave, Vancouver, BC, Canada, Phone: 604-675-8162; Fax: 604-675-8178, mmarra@bcgsc.ca. Michael D. Taylor, MD, PhD, FRCSC, 555 University Avenue, Toronto, Ontario, Canada, Phone: 416-813-6427 ; Fax: 416-813-4975, mdtaylor@sickkids.ca.
[*]These authors contributed equally.

Conflict of Interest: The authors declare no conflicts of interest.

Data Availability

The Gene Expression Omnibus accession numbers for the previously-unpublished gene expression data are GSE62802 (HGG samples) and GSE62803 (MB samples). The Toronto WES datasets are available under accession numbers EGAD00001000723 and EGAS00001001014.

Competing Financial Interests

The authors declare no competing financial interests.

Author contributions

A.S.M., F.M.G.C., M.R., M.D.T., and M.A.M. led the study and wrote the manuscript.
A.S.M and F.M.G.C. designed, supervised, and performed bioinformatic analyses. M.R. led collection of samples and data generation, and performed bioinformatics analyses. B.L. extracted nucleic acids, managed biobanking, and maintained the patient database. S.H., A.M.F., B.L.H., C.D., D.J.H.S., D.M.M., D.P., D.T.W.J., E.N.K., H.F., J.M., J.P., J.R., J.T., L.G., L.K.D., M.V., P.N., Sameer A., Steffen A., S.C.M., S.P-C., V.H., V.R., Xiaochong W., Xin W. and Y.Y.T. provided technical and bioinformatic support. A.A., A.T., C.M., D.L., E.C., E.M., H.I.L., J.E.S., K.T., M.M., N.D., P.P., R.C., R.D.C., T.W., W.L., Y.C., and Y.L. led and performed RNA-Seq and WGS library preparation and sequencing experiments and performed data analyses. N.T. and Y.M. supervised bioinformatics analyses at the Genome Sciences Center. H.N. and T.G. performed WES library preparation and sequencing experiments, and performed data analyses. A.H., A.J.M., A.K., D.M., E.B., G.D.B., J.T.R., M.K., P.D., P.L., R.A.M., S.J.M.J., S.M.P., U.T., provided valuable input regarding study design, data analysis, and interpretation of results. M.D.T. and M.A.M. provided financial and technical infrastructure and oversaw the study, and are joint senior authors and project co-leaders.

of monotherapy against a single target. Clinical trials of targeted therapies for medulloblastoma should first assure the spatially ubiquitous nature of the target mutation.

Letter

Many cancer types show considerable intertumoral heterogeneity between patients[1–3]. Molecular biomarkers are intended to (i) tailor treatment intensities[4,5], (ii) define oncogenic drivers for targeted therapies[5–7], and (iii) identify diagnostic mutations (i.e. *SMARCB1* in ATRT)[8]. Currently, clinical diagnoses are based on single biopsies due to the assumption of spatial homogeneity across tumors, however, spatial heterogeneity could lead to erroneous tumor classification, or selection of therapies against targets only present in a locally-restricted subset of the tumor. These implications were recently highlighted in late-stage renal cell carcinoma (RCC)[9,10] with highly divergent mutational profiles affecting *MTOR* and *TP53*, as well as demonstrating good and poor prognostic gene signatures in multi-region biopsies derived from the same tumor[10,11].

To determine the degree and clinical importance of spatial heterogeneity in medulloblastoma, we performed multi-regional biopsies and compared gene expression profiles, DNA copy number aberrations, and somatic mutations. Our cohort includes 9 primary medulloblastomas, 16 high-grade gliomas (HGG) (10 with gene expression only[12]), and 10 kidney cancers[10], each with 4–11 spatially distinct biopsies (median=6). An overview of the data types available for each patient is presented in Supplementary Table 1a and Supplementary Figure 1.

Glioblastoma[13] and medulloblastoma[14] each comprise four distinct molecular subgroups that are discerned through analysis of transcriptional data. Unsupervised hierarchical clustering (HCL) of expression data demonstrates that medulloblastoma biopsies form tight clusters apart from single samples[15–20] (8/8; Fig. 1a, Supplementary Fig. 2a–b), whereas in HGGs (3/3) and RCCs (8/9), multi-region biopsies from single individuals cluster apart when combined with single samples (Supplementary Fig. 2c–f,). Overall, based on the standard deviation of expression, inter-tumoral differences were greater than intra-tumoral heterogeneity in each tumor type (Fig. 1b). Using Predictive Analysis of Microarrays (PAM), subtype prediction revealed that 21% (13/63) of glioblastoma multi-region samples diverged from the most commonly observed subtype for each patient, compared to only 2% (1/52) of medulloblastoma biopsies (p=0.003; Fig. 1c–e; Supplementary Figs. 3–6). Considering only biopsies with subgroup predictions of 100% confidence, all MB tumors had concordant subgroup calls between multiple biopsies (9/9) compared to only 55% of glioblastomas (6/11; p=0.038; Fig. 1e). We conclude that medulloblastoma can be robustly and reliably sub-grouped from only a single biopsy, but glioblastoma cannot.

We identified somatic copy number aberrations (CNA) using a custom pipeline based on the TITAN algorithm[21], which is robust to high levels of normal contamination (see **Methods**). Regions of CNA were identified in all three tumor entities (Fig. 2a, Supplementary Fig. 7–8, Supplementary Table 1b–c), and unsupervised HCL of clonal segments showed tight clustering of individual biopsies in the cohort across all tumor entities (Fig. 2b, Supplementary Fig. 9). CNA-derived measurements of spatial heterogeneity reveal variance

between individuals within each tumor type (Fig. 2c). Somatic single nucleotide variants and indels recapitulate a similar pattern of spatial heterogeneity across tumors (Fig. 2d; Supplementary Table 1d). Overall, based on mutation and copy number data, none of the three tumor types were solely comprised of only homogeneous or heterogeneous tumors, rather, each have a repertoire of tumors that reside along a continuum of genetic heterogeneity.

This genomic complexity results from a process of clonal evolution whereby successive acquisition of mutations and copy number events generates genetically related subpopulations of cells or lineages within each tumor. We integrated CNA and mutational data using the EXPANDS algorithm[22], in order to infer the cellular lineage composition in each biopsy. EXPANDS detects multiple genetically distinct co-existing subpopulations of cells and allows phylogenetic reconstruction of their evolutionary relationships. A cartoon describing the spatial distribution of genetically distinct subpopulations throughout a tumor (Fig. 3a) illustrates the clonal intermixing detected in many samples of the cohort (Fig. 3b–d; Supplementary Fig. 10; Supplementary Table 1e–f). Many tumor biopsies have a major clone (genotype present in >70% of tumor cells) that is also detected in a minority of cells in other biopsies from the same tumor (i.e. are subclonal), or which is absent in other biopsies (e.g. biopsies 3,5,6 in RCC7 are genetically similar to some cells in biopsy 4 (4a), but not all cells, since 4b clusters separately; Fig. 3c). In some tumors, individual biopsies contain two or more cell lineages that independently accumulate distinct repertoires of mutations not found elsewhere in the tumor (e.g. HGG2 biopsies 1,5; Fig. 3c). The presence of multiple genetically distinct cellular lineages within single biopsies has previously been linked to poor prognosis and treatment response across a variety of cancer types[23].

This surprising but common pattern of major genetic clones in one biopsy that are subclonal or absent in spatially distinct locations in the tumor prompted us to investigate observable mutation clonality across biopsies, since clonality is a key requirement of clinically-actionable therapeutic targets[24]. We classified mutations into clonal and subclonal populations (Supplementary Fig. 11; Supplementary Table 1g), and determined whether the subset of damaging clonal mutations changes status between spatially-separated tumor biopsies. In nearly all tumors we find a predominance of clonal mutations that are subclonal or completely absent in additional biopsies (Fig. 4a; Supplementary Fig. 12; validation set of 7 mutations with 96% validation rate across biopsies; Supplementary Fig. 13 and Supplementary Table 1h). This observation remains true when considering only driver events[25,26,27,28] (Fig 4b; Supplementary Table 1i–k). We predict that monotherapies against a single target identified in a single biopsy are unlikely to show dramatic clinical effects as the targets are not ubiquitous, leaving untargeted clones in unsampled portions of the tumor free to survive and repopulate the tumor.

With the goal of improved patient treatment, the clinically relevant question is whether the observed level of genomic spatial heterogeneity affects actionable or driver alterations. As a proof of concept, we focused on a set of genes with known roles in cancer initiation/progression[29], or which have defined drug interactions[30]. These genes are therefore enriched in relevant or actionable targets in a manner unbiased towards either of the cancer types included (Supplementary Table 1l–m). Considering the spectrum of SNVs, indels, and

CNAs affecting these genes (Supplementary Fig. 14–15), we found a remarkable variety of patterns across tumors, including: cases with only a small set of shared alterations across biopsies but with many events present in single biopsies (e.g. HGG4 *MET* amplification); homogeneous tumors with many shared actionable events (e.g. HGG3); cases without ubiquitous actionable targets, which may require multi-agent targeted therapeutics (e.g. MB6); tumors lacking vulnerability to any of the considered actionable targets in a subset of biopsies (e.g. MB7); and tumors with alterations that may predict resistance (e.g. RCC7 *TP53* compound loss and somatic mutation).

Considering the full set of identified actionable mutations per tumor across all biopsies, we calculate that in each entity, an average of at least 5 biopsies are required to have an 80% chance of identifying at least 80% of these alterations. Lowering these measures to 50% would require sampling of at least 2 biopsies, with highly heterogeneous tumors needing as many as 4 (Fig. 5a). This is likely an underestimate, as the detection of actionable mutations does not plateau in most patients (Supplementary Fig. 16).

Upfront profiling of numerous tumor regions in order to reveal the full repertoire of actionable targets is neither practical nor likely, given the amount of sequencing required, thus we focused on maximizing the information derived from a minimal set of biopsies. Specifically, we wanted to determine how well we could predict the frequency of individual mutations across a tumor, given increasing number of biopsies, noting that prediction accuracy for mutations identified in a single fraction would be high only in very homogeneous tumors. We empirically determined the frequency of each alteration when considering all possible pairs of an increasing number of biopsies, and compared this observed quantity to the known frequency of the alteration in all biopsies; the difference between these values being the inference error of mutation frequency resulting from insufficient biopsies in genetically heterogeneous tumors (Supplementary Fig. 17). Taking a 10% error rate as an acceptable threshold, we calculate for each tumor the number of observed mutation frequencies that fall within this range (i.e. accuracy). As expected, accuracy improves with increasing number of biopsies, and also reveals that brain tumors fall into two patterns. The first comprises more homogeneous tumors, which have fairly high prediction accuracy even with a low number of biopsies, while the second comprises more heterogenous tumors that require multiple biopsies to ensure accurate determination of mutation frequency (Fig. 5b). In our cohort of medulloblastomas and glioblastomas, considering just two biopsies per tumor enables distinction of these high vs low genetic heterogeneity tumors, with high specificity especially for those tumors that are highly heterogeneous (Fig. 5c; Supplementary Fig. 18).

While spatial heterogeneity is clearly a barrier to highly effective therapeutics against the entire primary tumor, the extent of heterogeneity between a primary and recurrent medulloblastoma[31] is many fold greater (Fig. 6a, Supplementary Fig. 19). This vast discordance at relapse is therefore unlikely to be secondary solely to inadequate spatial sampling of the therapeutically-naïve primary tumor. In gliomas[32] the recurrent disease more closely resembles the primary and only in rare cases diverges to the extent seen in medulloblastoma, possibly due to less complete resection success in this more diffuse and infiltrating tumor. Medulloblastoma is known to recur from very rare populations of cells[31],

thus, therapeutic approaches that can eradicate such cellular lineages despite their low prevalence in the primary tumor are drastically needed.

Immunotherapy relies on the destruction of cancer cells based on the presence of tumor-specific cell-surface antigens as opposed to cell autonomous somatic mutations. We examined expression of the antigens/genes for which chimeric antigen receptor T-cells or monoclonal antibodies already exist[33–43], and demonstrate a remarkable consistency of expression across multi-regional biopsies, which contrasts highly to the inhomogeneity of somatic mutations across fractions in the same set of tumors. This was the case in all medulloblastomas examined, including those with high levels of genetic heterogeneity and in which targeted therapy would be problematic (Fig. 6b; Supplementary Fig. 20)[33–43]. Homogeneity of the transcriptome versus heterogeneity of somatic mutations in our MB cohort suggests that targeted immunotherapeutic approaches could overcome the hurdle of spatial genetic heterogeneity.

The vast majority of brain tumor patients have their tumor classified from a single tumor biopsy, which may be adequate for medulloblastoma, but not for glioblastoma patients. The extent of spatial heterogeneity of somatic mutations observed in our cohort suggests that clinical trials of molecularly targeted therapy should first assess the ubiquitous distribution of the target. The lack of clonal actionable driver mutations ubiquitously present across all regions of a given brain tumor suggest that monotherapies targeting a single gene from a single biopsy are unlikely to have dramatic effects to improve the lives of brain tumor patients.

Materials and Methods

Patients and samples

Multi-region tumor biopsies and clinical data were gathered for 35 tumors (9 primary medulloblastomas, 16 high-grade gliomas (HGG) (10 with gene expression only[12]), and 10 kidney cancers[10]); peripheral blood samples were included as germline (GL) controls for all cases with exome sequencing. All multi-region biopsies for unpublished cases were obtained in situ during tumor resection, by mimicking the previous sample preparation conditions of published cases to the best of our knowledge. Medulloblastoma tumors are similar in size to glioblastomas, with an average diameter of 8–12cm; biopsies were taken as far apart as possible by the surgeon. Renal cancers, due to their localization in the abdomen may be larger in size. Detailed information on multi-region tumor samples is provided in Supplementary Table 1a and Supplementary Figure 1. All patient material and clinical information were obtained after receiving informed consent and was approved by the institutional review boards of the contributing institutions. DNA and RNA extractions were performed as previously described[16]. RNA quality was assessed on a 2100 Bioanalyzer (Agilent Technologies, Santa Clara, CA). Only high-quality RNA (RNA integrity number ≥7) was included for further studies.

Gene expression profiling

Expression profiling was conducted on eight MB and three HGG multi-region biopsies totaling 72 biopsies with a median number of 6 multi-region biopsies per primary (range 4–9). Affymetrix HU133 Plus 2.0 microarrays were used for HGG samples and Affymetrix Gene 1.1 ST array (Affymetrix, Santa Clara, CA) was used for MB samples to ensure that these multi-region biopsies could be compared to published data sets[15–17,20]. Microarrays were processed according to the manufacturer's guidelines. Raw data was normalized using a transcript-level robust multi-array average (RMA) algorithm[44], and subsequently clustered using unsupervised HCL (Pearson's Dissimilarity – average linkage) in Partek Genomics Suite. The molecular classification of the multi-region biopsy samples was performed using a class prediction algorithm, Prediction Analysis for Microarrays (PAM)[45], as implemented in the pamr package (v 1.51). Markers for GBM subtypes were obtained from the Verhaak classifier[13]. We note that classification was performed for the GBM samples only, thus excluding HGG1. Subgroup-specific markers for MB were identified based on one-way analysis of variance (ANOVA) with multiple hypothesis correction by the Bonferroni method in previously published datasets with known subgroup affiliation[46]. Based on the misclassification error values in core GBM[13] and MB[15–17] training datasets (Supplementary Fig. 6), threshold values of 1.75 and 1 were chosen for multi-region samples from published[12] and unpublished GBM and MB patients, respectively. The published GBM dataset[12] was quantile normalized using Partek Genomics Suite. Predicted subtypes or subgroups with confidence probabilities higher than established thresholds[46] were considered bona fide subgroup assignments. Samples with less than 500 ng of remaining RNA were analyzed using NanoString as previously described[46]. MB3 was exclusively analyzed using NanoString since only limited amounts of RNA were available for all multi-region biopsies. NanoString counts were normalized to the three housekeeping genes (*GAPDH, ACTB* and *LDHA*). Dot plots and PCA based on normalized NanoString calls were prepared using the R-statistical environment (v2.15.1). Pearson correlation was used to determine the correlation of marker gene expression for each biopsy per patient (intra-tumor comparison) and between each biopsy and all others samples from different patients of the same subgroups (inter-tumor comparison). Wilcoxon rank sum test was used to infer intra- and inter-tumor marker gene expression differences in a subgroup-specific fashion.

A previously published dataset of nine multi-region RCC samples[9] profiled using the Affymetrix Human Gene 1.0 ST array was included in the analysis as well as two RCC datasets[18,19] with 53 and 29 single RCC samples, respectively. The RCC expression datasets have been processed together in R (v3.1.1) with the oligo package (rma normalization) and the combat package has been used for batch effect correction. Unsupervised HCL (Pearson's Dissimilarity – average linkage) has been performed using the Partek Genomics Suite.

The Gene Expression Omnibus accession numbers for the previously-unplublished gene expression data are GSE62802 (HGG samples) and GSE62803 (MB samples).

Whole-Exome Sequencing

DNA libraries (MB1-5) from multi-region samples were exome captured using Agilent SureSelect V5+UTR probes, followed by 8 cycles of PCR and then paired-end 75 base reads

were sequenced over 2 lanes on an Illumina HiSeq 2000 instrument per pool of 6 libraries. Reads were aligned to the human reference genome hg19a using the Burrows-Wheeler Aligner (BWA) (version 0.5.7)[47]. Two lanes were merged with duplicates marked using Picard Tools (version 1.71). Additional samples (MB6/7, HGG1-5) were subjected to paired-end library construction using Illumina's Nextera Rapid Capture Exome (RCE) kit. Captured exome DNA sequences were then sequenced on Illumina HiSeq 2000 (rapid-run mode) for 100-bp paired-end reads. We used FASTX toolkit to remove adaptor sequences and to trim low quality reads. Quality trimmed reads were then aligned to the human reference genome (hg19) using BWA (version 0.5.9)[47]. Genome Analysis Toolkit (GATK)[48] was used for indel realignment. Duplicate reads were then marked using Picard to be able to exclude them further in our analysis. The Toronto datasets are available under accession numbers EGAD00001000723 and EGAS00001001014.

Somatic SNV detection and filtering

SNVs were called exome-wide using samtools mpileup (v0.1.7), and indels were called using VarScan. Stringent filtering was performed requiring no reads in the germline sample supporting a SNV to ensure conservative selection of somatic events. Variants with sufficient coverage (≥10) were further annotated using Annovar[49] (table_annovar.pl; RefSeq gene annotations, amino acid change annotation, SIFT, PolyPhen, LRT, and MutationTaster scores, PhyloP and GERP++ conservation scores, dbSNP identifiers, 1000 Genomes Project allele frequencies, NHLBI-ESP 6500 exome project allele frequencies).

Mutation Validation

A subset of somatic mutations were validated using PCR amplification from all tumor biopsies, matched germline, and a healthy control sample. Regions of interest were amplified from genomic DNA using primers flanking each SNV (Supplementary Table 1h,n) using Q5 High-Fidelity DNA polymerase (NEB). PCR specificity was determined by agarose gel electrophoresis followed gel extraction of specific bands using Gel Extraction/PCR Clean-up kit (Qiagen) following manufacturer instructions. Purified amplicons were sequenced using Sanger sequencing, and traces reviewed manually for the expected presence or absence of the mutated base.

Droplet digital PCR

For the validation and quantification of the frequency of the PIK3CA SNV detected in MB3, we used droplet digital PCR (ddPCR), since Sanger traces were of poor quality in the region of interest. Genomic DNA from 6 spatially distinct biopsies from MB3 as well as matched germline and a healthy donor control were used in the assay. The PIK3CA mutation (chr 3:178936091 G>A) was validated by using the PrimePCR ddPCR mutation assay kit, PIK3CA p.E545K, human (Biorad, dHsaCP2000075 (mutant, FAM) and dHsaCP2000076 (Wt, VIC)), accordingly to manufacturer instructions. Fluorescence measurement using QX100 ddPCR droplet reader (Biorad) was used to detect the presence of mutant and wildtype alleles. QuantaSoft Analysis software (Biorad) was used in the quantification.

Copy number analysis

TITAN[21] estimates the cellular prevalence of tumor cell populations (lineages) based on a user-defined number of clonal clusters, and user-defined ploidy estimation. Thus, 20 runs of TITAN were performed for each exome, with cluster numbers 1 to 10 (representing one clonal lineage through to 10 co-existing clonal lineages with distinct genotypes), and ploidy set to either 2 or 4. Copy number segments from the 20 parameter combinations were analyzed and merged into larger segments if they were on the same chromosome arm, were <10Mb apart, and had the same state (loss or gain). Merged results from each of the 20 parameter combinations for each biopsy were compared in order to select the optimal parameter combination as the highest scoring considering the following criteria:

maximize the largest contig size

maximize the median contig size

minimize the number of contigs

minimize the number of clonal clusters

The parameter combination with the largest x value was selected as optimal, where:

$$x=((L*M)*(M^2/10^9)*(1/T)*(1/(C+1)^2))/M/10^9$$

L = largest contig size (Gb)

M = median contig size (Gb)

T = total number of contigs

C = clonal clusters

We next assessed the prevalence of copy number segments (loss or gain) identified in the best parameter combination of a unique biopsy (i.e. target segments), using either all segments or clonal segments only (logratio ≥ |0.2|). A target segment was considered as found in another biopsy from the same tumor if any of the 20 parameter combinations contained a segment with the same state (loss or gain), and whose span had a minimum reciprocal overlap of at least 70% with the target segment.

Concordance of driver regions of loss and gain in the RCC tumor cohort was performed for our calls and the published data[9]. With our computational approach, we achieved a 97% concordance when comparing to the manual curation performed previously[9], indicating that this method is specific and sensitive despite a high level of normal cell contamination in these tumors. Conversely, compared to our results for the subset of copy number gains and losses identified in Gerlinger *et al., 2014*, the manual curation shows an 89% concordance to the TITAN pipeline, indicating that our approach is more sensitive, and that the homogeneity of certain copy number driver events may be greater than previously estimated (Supplementary Table 1c). Finally, our approach is applicable genome-wide and across tumor types in a highly parallel fashion.

SNV Classification using mclust

Variant allele frequencies (VAF) of somatic SNVs were classified into distinct clusters using the R package mclust[50], which uses finite mixture estimation via iterative Expectation Maximization steps (EM) and the Bayesian Information Criterion (BIC). Each cluster is manually categorized as “homozygous”, “clonal”, or “subclonal”, depending on the cluster VAF and the uncertainty separating it from the next cluster, and taking into account the biopsy tumor cell content value reported by TITAN. Multiple subclonal populations are numbered sequentially, starting with the most highly prevalent population. Clonal and subclonal mutation details per biopsy are summarized in Supplementary Table 1d,g.

Phylogenetic reconstruction from combined SNV and CNV data

We combined copy number and LOH information derived from TITAN (including the clonal and subclonal events identified in the best parameter combination run for each biopsy), as well as somatic mutations and SNPs in areas of LOH, to infer tumor phylogenies using EXPANDS[22]. EXPANDS v1.7.2 was run with the runExPANdS function. All parameters were set to default with the exception of maxScore, which was lowered to 1.5 in order to reduce the false positive rate of subpopulation detection. Only subpopulations with a minimum size (cellular frequency) of 0.1 were considered. Mutations that could not be assigned to a high confidence subpopulation were discarded, so that no ambiguous assignments were made. In addition, ambiguous subpopulations (i.e. groups of mutations and copy number events) were dropped from the analysis. Mutations are assigned to all nested subpopulations (i.e. if a mutation is found in a subpopulation of cells at a high frequency of 0.8, it will also be assigned to “daughter” subpopulations, for instance of frequency 0.5), to report the assignment of every mutation to all detected subpopulations in all biopsies of the tumor (assuming that the mutation could be assigned unambiguously as mentioned above; Supplementary Table 1f).

Phylogenetic relationships between the subpopulations inferred by the EXPANDS algorithm in all biopsies per patient were generated using both SNV and copy number segments. The Manhattan distance metric was used to calculate pairwise distances between all pairs of biopsies based on this data, and a complete linkage hierarchical clustering was performed to generate phylogenies. Germline-rooted trees were generated using the as.phylo R function from the ape package.

Error inference of actionable genetic alterations

In order to perform an analysis of genetic heterogeneity affecting actionable and putative driver genes in a way that is unbiased to either of the tumor types, we opted to use general lists of known cancer drivers and drugable genes. Sets of genes known to be drivers in GBM, MB, and RCC tumors come from studies of different cohort sizes, with sometimes unknown subgroup affiliation, and thus are not equally comprehensive. To overcome this, we used a list of genes of interest that includes putative driver genes found in the Cancer Gene Census database[29] (n=572) and actionable genes from the Drug-Gene Interaction Database[30] (n=426 genes) (Supplementary Table 1l–m).

Oncoprint plots (R package ComplexHeatmap v1.6.0) were built for the combination list of these genes for all tumors, using (a) clonal mutations and indels and (b) clonal mutations and indels plus high-level copy number aberrations (>4 copies gained; homozygous loss). Manual review of results revealed that absence of clonal somatic mutations in subsets of biopsies is not explained by concordant copy number loss. Since not all biopsies had copy number data, further analyses were performed using results from strategy (a) in order to maximize the number of usable biopsies per tumor.

Driver event lists

The MB CNA driver events in Supplementary Table 1i,j and Figure 4b are mainly taken from Shih *et al.*[27] plus a subset of the mostly highly recurrent genes listed in Northcott *et al.*[25]. The HGG chromosome arm and recurrent driver genes events were retrieved from Sturm *et al.*[26] (Table 1 and 2 of Reference 26). RCC chromosome arm and gene-level driver events were retrieved from the ccRCC TCGA paper[28] (Sup Fig 22 threshold FDR q-value< 10^{-15} and Table S4, q-value threshold 0.05). Cancer cell fraction values presented in Supplementary Figure 10b for driver mutations were calculated as previously described[51]:

$$\mathrm{CCF}=\mathrm{VAF}*(1/\mathrm{purity})(\mathrm{CN}*\mathrm{purity}+2(1-\ \mathrm{purity}))$$

where CCF=cancer cell fraction, VAF=variant allele frequency, CN=copy number at the mutation, purity=tumor purity as calculated by EXPANDS.

Accuracy of mutation frequency detection

We calculate the inferred error of the prevalence of each mutation across biopsies using a subsampling approach. In each tumor, given a subset of biopsies from 1 to n (where n = total biopsies per tumor), the frequency of each identified mutation in the biopsies sampled is calculated as $f_{o.}$ This value is subtracted from the “ground truth” expected frequency for that mutation across all n biopsies (f_e). When the observed and expected values are identical, then the inferred error ($f_e - f_o$) is 0. In the majority of tumors, there is a predominance of genes with mutations in single biopsies, leading to negative values of error for many genes as the frequency of the mutation is often overestimated (Supplemental Fig. 17). In contrast, genes that are present in all but one or two biopsies will often have an error value over 0, as their frequency can be underestimated.

The likelihood of being within $^{+/-}0.1$ of 0 (i.e. close to perfect accuracy given the data from all biopsies) is calculated as the proportion of genes at each sampling of 1:n biopsies where the error rate was within those bounds. For instance, we sample all possible combinations of a certain number of biopsies from the total number of biopsies, and in each case calculate the inferred error of each detected mutation’s prevalence. The proportion of the total set of error values < |0.1| is the likelihood of a correct interpretation of mutation frequency given that number of biopsies (Fig. 5b).

Genetic heterogeneity estimation from two biopsies

To address the practical issue of estimating genetic heterogeneity from a minimum number of informative biopsies, we implemented a simple metric of the proportion of mutated genes

in a set of 2 biopsies that was ubiquitous (i.e. present in 2 of 2 biopsies). The mean value of all pairs of biopsies from a total of n biopsies per tumor showed a strong divergence in HGG and MB tumors, with high- vs low-variability tumors well separated (Fig. 5c). These were the same tumors that scored as high vs low variability based on the accuracy metric described above.

We also observed clear separation of these two classes using the R package mclust (Supplementary Fig. 18a), which models univariate mixtures of Gaussian distributions (i.e. corresponding to a mixture of high and low genetic variance brain tumors) via Expectation-Maximization and the Bayesian Information Criterion[50]. Choosing two thresholds from the mclust density peaks (low=0.55, high=0.75), we calculated the accuracy of classifying high-variance vs low-variance tumors based on a single pair of biopsies, and observed that high-variance tumors in particular have a high true positive and low false positive classification rate (Supplementary Figure 18b). I.e. based on this metric, the vast majority of pairs of biopsies from tumors with high genetic heterogeneity have a low percentage of gene mutations found in both biopsies, such that they are always classified as heterogeneous tumors, and almost never as homogeneous tumors.

Expression analysis of immunotherapeutic targets in MB tumors

Microarray expression data from the Affymetrix Gene 1.1 ST array (Affymetrix, Santa Clara, CA) for the MB samples were analyzed in the R environment (v3.1.1).

We used the affy package (v1.44.0) and the custom CDF hugene11sthsensgcdf (v19.0.0) to summarize the expression of 21641 Ensembl (ENSG) genes and process the data. Expression data was normalized using the rma method.

Spatial genetic variance vs post-treatment clonal evolution

To directly measure the relative contribution of spatial heterogeneity versus clonal evolution induced by treatment, we utilized our previously published cohort of matched pre- and post-therapeutic MB samples[31]. This comparison shows that in MB, the amount of divergence observed between primary and relapse compartments far exceeds spatial genetic variance in the primary tumor.

To assess whether the observed divergence between primary and recurrent MB is greater than the observed divergence between intra-tumoral biopsies, we re-analyzed the 14 primary-relapse tumor WGS samples with matched germline using the same pipeline as presented above. Briefly, mutations were called using samtools mpileup, filtered stringently against the germline, and shortlisted to those mutations that have at least 10 reads coverage in both the primary and recurrent samples, and are in areas of normal copy number and LOH. Since the samples in this work are exomes, we restricted the analysis of the primary-relapse samples to the same exonic regions. After removing the major analysis pipeline differences, we addressed differences in depth of coverage. The exome libraries were sequenced to an average of 60X, while the WGS samples were sequenced to 30X coverage. Thus, our ability to assess similarity between regions in the exome libraries is more sensitive to subclonal events present at low levels (and therefore preferentially detectable by exome seq and not by WGS). We addressed this bias by restricting the analysis to clonal events in

the exomes, as clonal mutations are detectable both in exomes and genomes. To verify that this was a reasonable assumption, we compared the VAF of mutations found in the exomes to those found in matched WGS data generated from the same samples, but sequenced at 30X coverage. Matched WGS samples are available for biopsy 1 in each MB tumor with multi-regional profiling. In all cases, we found that >75% of mutations with a VAF < 0.18 in the MB exomes were not found in the matched genomes sequenced from the same samples, indicating that subclonal events are typically not well profiled at the shallower depths of a genomic library. Therefore we restricted our analysis to clonal events in both the exomes and genomes.

Focusing on the clonal and homozygous events detectable in both exome and genome data, we hypothesized that any differences between primary and relapse samples that are greater than the differences expected from different biopsies in a primary tumor would be largely attributable to clonal evolution as a consequence of therapy. To see if the data support this conclusion, we used the mutations in each biopsy to measure pairwise concordance between all biopsies of individual tumors. Concordance is measured as the number of mutations in common between two biopsies, as a fraction of the total number of mutations present in both. In parallel, we used the mutations in the primary and relapse samples to measure pairwise concordance values between disease compartments. As a positive control, we compared the inter-biopsy and inter-compartmental concordance values of an adult GBM sample with multiple biopsies profiled before and after therapy (Patient 17 from reference[32]).

In MB samples we found a mean pairwise concordance of 0.3903 between biopsies of the same tumor, nearly an order of magnitude higher than the mean concordance (0.03852) observed between disease compartments (Wilcoxon Rank Sum test p-value < 2.2e–16). One sample stood out as an outlier (MB-REC-04), and we note that in this case the tumor was a Group4 local recurrence. This unusual pattern of recurrence for a Group4 tumor may indicate that the primary mass was sub-totally resected rather than grossly resected, explaining the higher similarity of the recurrent compartment to the primary.

In the case of the adult GBM patient (Patient17) with multi-regionally sampled primary (3 regions; low-grade glioma) and recurrent disease (4 regions; high-grade glioma), we found the same trend: the primary-relapse mean concordance of 0.01506 was an order of magnitude smaller than the mean intra-biopsy concordance of 0.5036 (Wilcoxon Rank Sum test p-value = 0.0001406). There was no significant difference between the primary-relapse MB concordance and the primary-relapse GBM concordance observed in Patient17 (Wilcoxon Rank Sum test p-value = 0.5458). Similarly, there was no significant difference between the regional biopsies in GBM vs MB (Wilcoxon Rank Sum test p-value = 0.09926).

Finally, the primary-relapse divergence calculated using reprocessed data from Patient17 was on par with that initially presented in the glioma paper[41], thus we included, for visual comparison, all the primary-relapse values for the glioma cohort in Figure 6a (middle panel; Johnson *et al*, 2014; values directly derived from Supplementary Table 4[32]).

Statistical analysis

All statistical analyses were performed in the R statistical environment. Comparisons of categorical variables between entity types were performed using the two-sided Fisher's exact test. Comparisons of distributions were performed using the Welch two-sample t-test (parametric) or the Wilcoxon Rank Sum test (non-parametric). P-values <0.05 were considered statistically significant.

Supplementary Material

Refer to Web version on PubMed Central for supplementary material.

Authors

A Sorana Morrissy[1,2,*], Florence MG Cavalli[1,2,*], Marc Remke[1,2,3,4,5,*], Vijay Ramaswamy[1,2,6], David JH Shih[1,2,7], Borja L Holgado[1,2], Hamza Farooq[1,2,7], Laura K Donovan[1,2], Livia Garzia[1,2,8], Sameer Agnihotri[9], Erin N Kiehna[10], Eloi Mercier[11], Chelsea Mayoh[11], Simon Papillon-Cavanagh[12], Hamid Nikbakht[12], Tenzin Gayden[12], Jonathon Torchia[2,6,7], Daniel Picard[3,4,5], Diana M Merino[2,6], Betty Luu[1,2], Xiaochong Wu[1,2], Stuart Horswell[14], Yuan Yao Thompson[1,2,7], Volker Hovestadt[15], Paul A Northcott[16], David TW Jones[16], John Peacock[1,2,7], Xin Wang[1,2,7], Stephen C Mack[1,2,7], Juri Reimand[17,18,19], Steffen Albrecht[20], Adam M Fontebasso[21], Nina Thiessen[11], Yisu Li[11], Jacqueline E Schein[11], Darlene Lee[11], Rebecca Carlsen[11], Michael Mayo[11], Kane Tse[11], Angela Tam[11], Noreen Dhalla[11], Adrian Ally[11], Eric Chuah[11], Young Cheng[11], Patrick Plettner[11], Haiyan I Li[11], Richard D Corbett[11], Tina Wong[11], William Long[11], James Loukides[2], Pawel Buczkowicz[22], Cynthia E Hawkins[2,22], Uri Tabori[2,6], Brian R Rood[23], John S Myseros[24], Roger J Packer[25], Andrey Korshunov[26], Peter Lichter[15,27], Marcel Kool[16], Stefan M Pfister[16,27,28], Ulrich Schüller[29,30,31], Peter Dirks[2,10], Annie Huang[2,6], Eric Bouffet[2,6], James T Rutka[2,7,10], Gary D Bader[19], Charles Swanton[32,33], Yusanne Ma[11], Richard A Moore[11], Andrew J Mungall[11], Jacek Majewski[21], Steven JM Jones[11,34,35], Sunit Das[1,2,36], David Malkin[6], Nada Jabado[21], Marco A Marra[11,34,#], and Michael D Taylor[1,2,7,#]

Affiliations

[1]Developmental & Stem Cell Biology Program, The Hospital for Sick Children, Toronto, Ontario, Canada

[2]The Arthur and Sonia Labatt Brain Tumour Research Centre, The Hospital for Sick Children, Toronto, Ontario, Canada

[3]Department of Pediatric Oncology, Hematology, and Clinical Immunology, Medical Faculty, University Hospital Düsseldorf, Düsseldorf, Germany

[4]Department of Neuropathology, Medical Faculty, University Hospital Düsseldorf, Düsseldorf, Germany

[5]Department of Pediatric Neuro-Oncogenomics, German Cancer Consortium (DKTK) and German Cancer Research Center (DKFZ), Düsseldorf, Germany

[6]Division of Haematology / Oncology, Department of Pediatrics, The Hospital for Sick Children, Toronto, Ontario, Canada

[7]Department of Laboratory Medicine and Pathobiology, University of Toronto, Toronto, Ontario, Canada

[8]Cancer Research Program, McGill University Health Centre Research Institute, Montreal, Quebec, Canada

[9]MacFeeters-Hamilton Brain Tumour Centre, Princess Margaret Cancer Centre, University Health Network, Toronto, Ontario, Canada

[10]Division of Neurosurgery, The Hospital for Sick Children, Toronto, Ontario, Canada

[11]Canada's Michael Smith Genome Sciences Centre, BC Cancer Agency, Vancouver, British Columbia, Canada

[12]Departments of Pediatrics and Human Genetics, McGill University, Montreal, Quebec, Canada

[13]Program in Genetics and Genome Biology, The Hospital for Sick Children, Toronto, Ontario, Canada

[14]Cancer Research UK London Research Institute, London, United Kingdom

[15]Division of Molecular Genetics, German Cancer Research Center (DKFZ), Heidelberg, Germany

[16]Division of Pediatric Neurooncology, German Cancer Research Center (DKFZ), Heidelberg, Germany

[17]Informatics and Biocomputing, Ontario Institute for Cancer Research, Toronto, Ontario, Canada

[18]Department of Medical Biophysics, University of Toronto, Toronto, Ontario, Canada

[19]The Donnelly Centre, University of Toronto, Toronto, Ontario, Canada

[20]Department of Pathology, Montreal Children's Hospital, McGill University Health Centre, Montreal, QC, Canada

[21]Division of Experimental Medicine, McGill University, Montreal, Quebec, Canada

[22]Division of Pathology, The Hospital for Sick Children, Toronto, Ontario, Canada

[23]Division of Pediatric Oncology, Children's National Medical Center, Washington DC, United States

[24]Division of Pediatric Neuro-Surgery, Children's National Medical Center, Washington DC, United States

[25]Department of Neurology, Children's National Medical Center, Washington DC, United States

[26]Clinical Cooperation Unit Neuropathology, German Cancer Research Center (DKFZ), Heidelberg, Germany

[27]German Cancer Consortium (DKTK), Germany

[28]Department of Pediatric Oncology, Hematology, Immunology and Pulmonology, University Hospital Heidelberg, Heidelberg, Germany

[29]Institute of Neuropathology, University Medical Center, Hamburg-Eppendorf, Germany

[30]Research Institute Children's Cancer Center, Hamburg, Germany

[31]Pediatric Hematology and Oncology, University Medical Center, Hamburg-Eppendorf, Germany

[32]Translational Cancer Therapeutics Laboratory, The Francis Crick Institute, London, United Kingdom

[33]Cancer Research UK Lung Cancer Centre of Excellence, University College, London, United Kingdom

[34]Department of Medical Genetics, University of British Columbia, Vancouver, British Columbia, Canada

[35]Department of Molecular Biology & Biochemistry, Simon Fraser University, Burnaby, British Columbia, Canada

[36]Division of Neurosurgery, St Michael's Hospital, University of Toronto, Toronto, Ontario, Canada

Acknowledgments

The MAGIC project is financially supported by: Genome Canada, Genome BC, Terry Fox Research Institute, Ontario Institute for Cancer Research, Pediatric Oncology Group Ontario, Funds from 'The Family of Kathleen Lorette' and the Clark H. Smith Brain Tumour Centre, Montreal Children's Hospital Foundation, Hospital for Sick Children: Sonia and Arthur Labatt Brain Tumour Research Centre, Chief of Research Fund, Cancer Genetics Program, Garron Family Cancer Centre, B.R.A.I.N. Child, M.D.T.'s Garron Family Endowment, and BC Childhood Cancer Parents Association. M.D.T. is also supported by a Stand Up To Cancer − St. Baldrick's Pediatric Dream Team Translational Research Grant (SU2C-AACR-DT1113). Stand Up To Cancer is a program of the Entertainment Industry Foundation administered by the American Association for Cancer Research. M.D.T. is supported by The Garron Family Chair in Childhood Cancer Research, and grants from the Cure Search Foundation, the National Institutes of Health (R01CA148699 and R01CA159859), The Pediatric Brain Tumor Foundation, The Terry Fox Research Institute, and Brainchild. This study was conducted with the support of the Ontario Institute for Cancer Research through funding provided by the Government of Ontario, as well as The Brain Tumour Foundation of Canada Impact Grant of the Canadian Cancer Society and Brain Canada with the financial assistance of Health Canada (grant #703202). This work was also supported by a Program Project Grant from the Terry Fox Research Institute, and a Grand Challenge Award from CureSearch for Children's Cancer. Additionally, this work was supported by the PedBrain Tumor Project contributing to the International Cancer Genome Consortium, funded by German Cancer Aid (109252) and by the German Federal Ministry of Education and Research (BMBF, grants 01KU1201A and MedSys 0315416C). We wish to acknowledge the Labatt Brain Tumour Research Centre Tumour and Tissue Repository, which is supported by B.R.A.I.N. Child and Megan's Walk. M.A.M. wishes to acknowledge support from the Canadian Institutes of Health Research (CIHR; FDN-143288). M.R. is supported by a fellowship from the Dr. Mildred Scheel Foundation for Cancer Research/ German Cancer Aid. F.M.G.C. is supported by the Stephen Buttrum Brain Tumour Research Fellowship, granted by Brain Tumour Foundation of Canada. V.R. is supported by a CIHR fellowship and an Alberta Innovates-Health Solutions Clinical Fellowship. For technical support and expertise of next-generation sequencing efforts we thank The Centre for Applied Genomics (Toronto). We thank S. Archer for technical writing and C. Smith for artwork.

References

1. Northcott PA, et al. Medulloblastoma Comprises Four Distinct Molecular Variants. J Clin Oncol. 2011; 29:1408–1414. DOI: 10.1200/JCO.2009.27.4324 [PubMed: 20823417]
2. Kleinman CL, et al. Fusion of TTYH1 with the C19MC microRNA cluster drives expression of a brain-specific DNMT3B isoform in the embryonal brain tumor ETMR. Nature genetics. 2014; 46:39–44. DOI: 10.1038/ng.2849 [PubMed: 24316981]
3. Versteege I, et al. Truncating mutations of hSNF5/INI1 in aggressive paediatric cancer. Nature. 1998; 394:203–206. DOI: 10.1038/28212 [PubMed: 9671307]
4. Pietsch T, et al. Prognostic significance of clinical, histopathological, and molecular characteristics of medulloblastomas in the prospective HIT2000 multicenter clinical trial cohort. Acta neuropathologica. 2014
5. Remke M, Ramaswamy V, Taylor MD. Medulloblastoma molecular dissection: the way toward targeted therapy. Current opinion in oncology. 2013; 25:674–681. DOI: 10.1097/CCO.0000000000000008 [PubMed: 24076581]
6. Kool M, et al. Genome sequencing of SHH medulloblastoma predicts genotype-related response to smoothened inhibition. Cancer cell. 2014; 25:393–405. DOI: 10.1016/j.ccr.2014.02.004 [PubMed: 24651015]
7. Kieran MW. Targeted treatment for sonic hedgehog-dependent medulloblastoma. Neuro-oncology. 2014; 16:1037–1047. DOI: 10.1093/neuonc/nou109 [PubMed: 24951114]
8. Louis DN, et al. The 2007 WHO classification of tumours of the central nervous system. Acta neuropathologica. 2007; 114:97–109. DOI: 10.1007/s00401-007-0243-4 [PubMed: 17618441]
9. Gerlinger M, et al. Genomic architecture and evolution of clear cell renal cell carcinomas defined by multiregion sequencing. Nature genetics. 2014; 46:225–233. DOI: 10.1038/ng.2891 [PubMed: 24487277]
10. Gerlinger M, et al. Intratumor heterogeneity and branched evolution revealed by multiregion sequencing. The New England journal of medicine. 2012; 366:883–892. DOI: 10.1056/NEJMoa1113205 [PubMed: 22397650]
11. Gulati S, et al. Systematic Evaluation of the Prognostic Impact and Intratumour Heterogeneity of Clear Cell Renal Cell Carcinoma Biomarkers. European urology. 2014
12. Sottoriva A, et al. Intratumor heterogeneity in human glioblastoma reflects cancer evolutionary dynamics. Proceedings of the National Academy of Sciences of the United States of America. 2013; 110:4009–4014. DOI: 10.1073/pnas.1219747110 [PubMed: 23412337]
13. Verhaak RG, et al. Integrated genomic analysis identifies clinically relevant subtypes of glioblastoma characterized by abnormalities in PDGFRA, IDH1, EGFR, and NF1. Cancer cell. 2010; 17:98–110. S1535-6108(09)00432-2 [pii]. DOI: 10.1016/j.ccr.2009.12.020 [PubMed: 20129251]
14. Taylor MD, et al. Molecular subgroups of medulloblastoma: the current consensus. Acta neuropathologica. 2012; 123:465–472. DOI: 10.1007/s00401-011-0922-z [PubMed: 22134537]
15. Northcott PA, et al. Enhancer hijacking activates GFI1 family oncogenes in medulloblastoma. Nature. 2014; 511:428–434. DOI: 10.1038/nature13379 [PubMed: 25043047]
16. Northcott PA, et al. Subgroup-specific structural variation across 1,000 medulloblastoma genomes. Nature. 2012; 488:49–56. DOI: 10.1038/nature11327 [PubMed: 22832581]
17. Vanner RJ, et al. Quiescent sox2(+) cells drive hierarchical growth and relapse in sonic hedgehog subgroup medulloblastoma. Cancer cell. 2014; 26:33–47. DOI: 10.1016/j.ccr.2014.05.005 [PubMed: 24954133]
18. Beuselinck B, et al. Molecular subtypes of clear cell renal cell carcinoma are associated with sunitinib response in the metastatic setting. Clinical cancer research : an official journal of the American Association for Cancer Research. 2015; 21:1329–1339. DOI: 10.1158/1078-0432.ccr-14-1128 [PubMed: 25583177]
19. Thibodeau BJ, et al. Characterization of clear cell renal cell carcinoma by gene expression profiling. Urologic oncology. 2016; 34:168 e161–169. DOI: 10.1016/j.urolonc.2015.11.001

20. Gravendeel LA, et al. Intrinsic gene expression profiles of gliomas are a better predictor of survival than histology. Cancer research. 2009; 69:9065–9072. DOI: 10.1158/0008-5472.can-09-2307 [PubMed: 19920198]
21. Ha G, et al. TITAN: inference of copy number architectures in clonal cell populations from tumor whole-genome sequence data. Genome research. 2014; 24:1881–1893. DOI: 10.1101/gr.180281.114 [PubMed: 25060187]
22. Andor N, Harness JV, Muller S, Mewes HW, Petritsch C. EXPANDS: expanding ploidy and allele frequency on nested subpopulations. Bioinformatics. 2014; 30:50–60. DOI: 10.1093/bioinformatics/btt622 [PubMed: 24177718]
23. Andor N, et al. Pan-cancer analysis of the extent and consequences of intratumor heterogeneity. Nature medicine. 2016; 22:105–113. DOI: 10.1038/nm.3984
24. Hiley C, de Bruin EC, McGranahan N, Swanton C. Deciphering intratumor heterogeneity and temporal acquisition of driver events to refine precision medicine. Genome biology. 2014; 15:453. [PubMed: 25222836]
25. Northcott PA, et al. Medulloblastomics: the end of the beginning. Nature reviews. Cancer. 2012; 12:818–834. DOI: 10.1038/nrc3410 [PubMed: 23175120]
26. Sturm D, et al. Paediatric and adult glioblastoma: multiform (epi)genomic culprits emerge. Nature reviews. Cancer. 2014; 14:92–107. DOI: 10.1038/nrc3655 [PubMed: 24457416]
27. Shih DJ, et al. Cytogenetic prognostication within medulloblastoma subgroups. J Clin Oncol. 2014; 32:886–896. DOI: 10.1200/jco.2013.50.9539 [PubMed: 24493713]
28. Linehan WM, et al. Comprehensive Molecular Characterization of Papillary Renal-Cell Carcinoma. The New England journal of medicine. 2016; 374:135–145. DOI: 10.1056/NEJMoa1505917 [PubMed: 26536169]
29. Futreal PA, et al. A census of human cancer genes. Nature reviews. Cancer. 2004; 4:177–183. DOI: 10.1038/nrc1299 [PubMed: 14993899]
30. Griffith M, et al. DGIdb: mining the druggable genome. Nature methods. 2013; 10:1209–1210. DOI: 10.1038/nmeth.2689 [PubMed: 24122041]
31. Morrissy AS, et al. Divergent clonal selection dominates medulloblastoma at recurrence. Nature. 2016; 529:351–357. DOI: 10.1038/nature16478 [PubMed: 26760213]
32. Johnson BE, et al. Mutational analysis reveals the origin and therapy-driven evolution of recurrent glioma. Science. 2014; 343:189–193. DOI: 10.1126/science.1239947 [PubMed: 24336570]
33. Geldres C, et al. T lymphocytes redirected against the chondroitin sulfate proteoglycan-4 control the growth of multiple solid tumors both in vitro and in vivo. Clinical cancer research : an official journal of the American Association for Cancer Research. 2014; 20:962–971. DOI: 10.1158/1078-0432.ccr-13-2218 [PubMed: 24334762]
34. Stein R, et al. CD74: a new candidate target for the immunotherapy of B-cell neoplasms. Clinical cancer research : an official journal of the American Association for Cancer Research. 2007; 13:5556s–5563s. DOI: 10.1158/1078-0432.ccr-07-1167 [PubMed: 17875789]
35. Wu MR, Zhang T, DeMars LR, Sentman CL. B7H6-specific chimeric antigen receptors lead to tumor elimination and host antitumor immunity. Gene therapy. 2015; 22:675–684. DOI: 10.1038/gt.2015.29 [PubMed: 25830550]
36. Chinnasamy D, et al. Gene therapy using genetically modified lymphocytes targeting VEGFR-2 inhibits the growth of vascularized syngenic tumors in mice. The Journal of clinical investigation. 2010; 120:3953–3968. DOI: 10.1172/jci43490 [PubMed: 20978347]
37. Craddock JA, et al. Enhanced tumor trafficking of GD2 chimeric antigen receptor T cells by expression of the chemokine receptor CCR2b. Journal of immunotherapy (Hagerstown, Md : 1997). 2010; 33:780–788. DOI: 10.1097/CJI.0b013e3181ee6675
38. Hong H, et al. Diverse solid tumors expressing a restricted epitope of L1-CAM can be targeted by chimeric antigen receptor redirected T lymphocytes. Journal of immunotherapy (Hagerstown, Md : 1997). 2014; 37:93–104. DOI: 10.1097/cji.0000000000000018
39. Kakarla S, et al. Antitumor effects of chimeric receptor engineered human T cells directed to tumor stroma. Molecular therapy : the journal of the American Society of Gene Therapy. 2013; 21:1611–1620. DOI: 10.1038/mt.2013.110 [PubMed: 23732988]

40. Lanitis E, et al. Primary human ovarian epithelial cancer cells broadly express HER2 at immunologically-detectable levels. PloS one. 2012; 7:e49829. [PubMed: 23189165]
41. Pule MA, et al. Virus-specific T cells engineered to coexpress tumor-specific receptors: persistence and antitumor activity in individuals with neuroblastoma. Nature medicine. 2008; 14:1264–1270. DOI: 10.1038/nm.1882
42. Tang X, et al. T cells expressing a LMP1-specific chimeric antigen receptor mediate antitumor effects against LMP1-positive nasopharyngeal carcinoma cells in vitro and in vivo. Journal of biomedical research. 2014; 28:468–475. DOI: 10.7555/jbr.28.20140066 [PubMed: 25469116]
43. Wang W, et al. Specificity redirection by CAR with human VEGFR-1 affinity endows T lymphocytes with tumor-killing ability and anti-angiogenic potency. Gene therapy. 2013; 20:970–978. DOI: 10.1038/gt.2013.19 [PubMed: 23636245]
44. Irizarry RA, et al. Summaries of Affymetrix GeneChip probe level data. Nucleic acids research. 2003; 31:e15. [PubMed: 12582260]
45. Tibshirani R, Hastie T, Narasimhan B, Chu G. Diagnosis of multiple cancer types by shrunken centroids of gene expression. Proceedings of the National Academy of Sciences of the United States of America. 2002; 99:6567–6572. DOI: 10.1073/pnas.082099299 [PubMed: 12011421]
46. Northcott PA, et al. Rapid, reliable, and reproducible molecular sub-grouping of clinical medulloblastoma samples. Acta neuropathologica. 2012; 123:615–626. DOI: 10.1007/s00401-011-0899-7 [PubMed: 22057785]
47. Li H, Durbin R. Fast and accurate short read alignment with Burrows-Wheeler transform. Bioinformatics. 2009; 25:1754–1760. DOI: 10.1093/bioinformatics/btp324 [PubMed: 19451168]
48. McKenna A, et al. The Genome Analysis Toolkit: a MapReduce framework for analyzing next-generation DNA sequencing data. Genome research. 2010; 20:1297–1303. DOI: 10.1101/gr.107524.110 [PubMed: 20644199]
49. Wang K, Li M, Hakonarson H. ANNOVAR: functional annotation of genetic variants from high-throughput sequencing data. Nucleic acids research. 2010; 38:e164. [PubMed: 20601685]
50. Fraley, CRM., TB, Scrucca, L. mclust Version 4 for R: Normal Mixture Modeling for Model-Based Clustering, Classification, and Density Estimation. University of Washington; 2012.
51. Stephens PJ, et al. The landscape of cancer genes and mutational processes in breast cancer. Nature. 2012; 486:400–404. DOI: 10.1038/nature11017 [PubMed: 22722201]

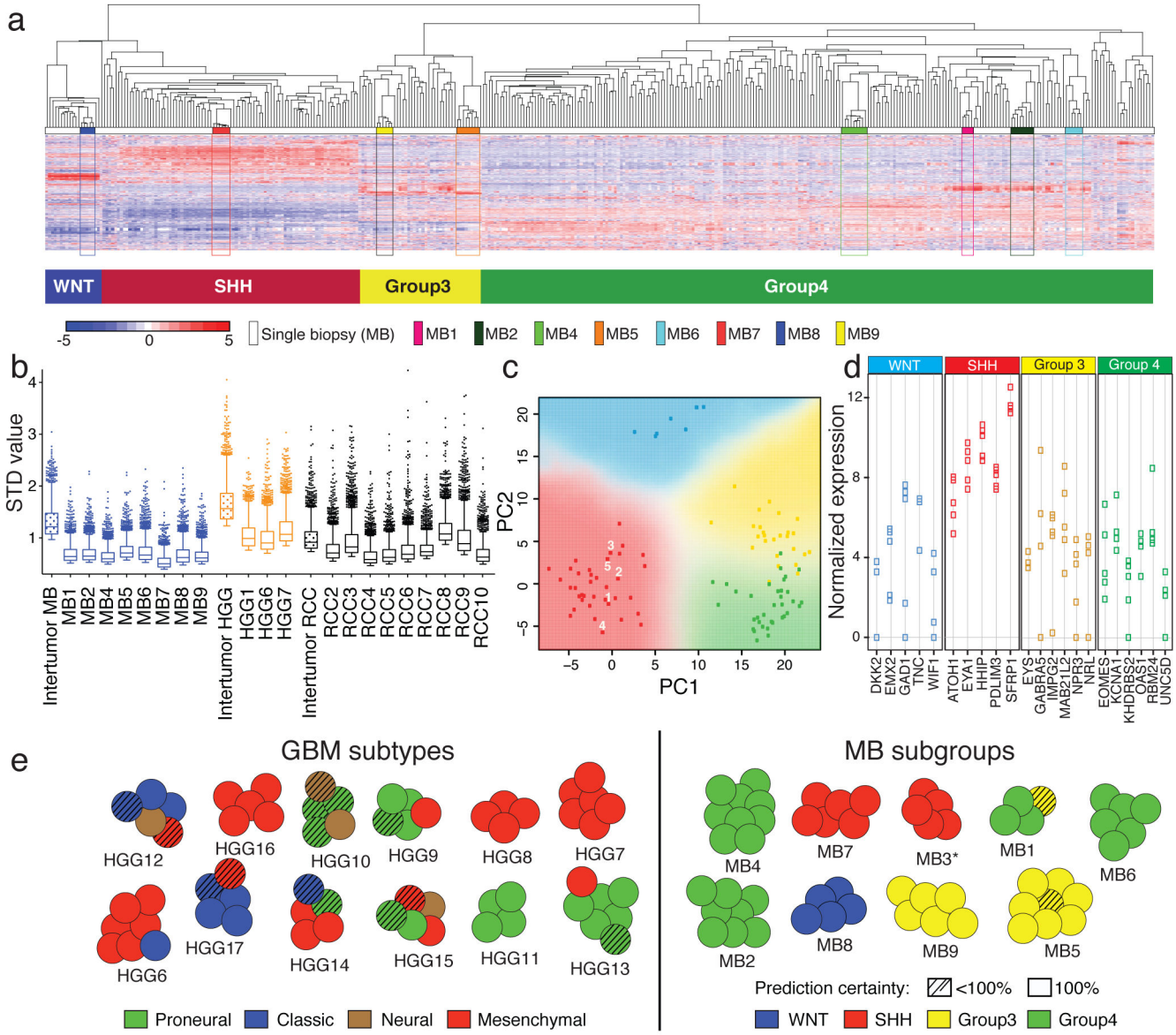

Figure 1. Medulloblastomas, but not glioblastomas, show reliable transcriptome-based subgroup prediction

(**a**) Unsupervised HCL using 1,000 high–SD transcripts of eight multi-region medulloblastoma (MB) samples combined with single biopsies (n=334) demonstrates tight clustering of matched multi-region MB samples across subgroups. (**b**) Box plot of the top 2000 SD-transcript values determined on an intra- and inter-tumor level in MB, HGG and RCC. **(c)** Principal component analysis (PCA) using 22 MB subgroup marker genes confirms a low degree of transcriptional intra-tumoral heterogeneity exemplified in MB3. Multi-region biopsy numbers of MB3 are indicated, and PCA was conducted with 103 single biopsy samples analyzed by NanoString. (**d**) Dot plot illustrating highly comparable marker gene expression in all multi-region biopsies for MB3. (**e**) Illustration showing GBM subtype and MB subgroup predictions based on Predictive Analysis of Microarrays (PAM) results.

SHH subgroup affiliation of MB3 (marked with a *) was inferred based on NanoString results. Hashed circles are biopsies with <100% prediction confidence.

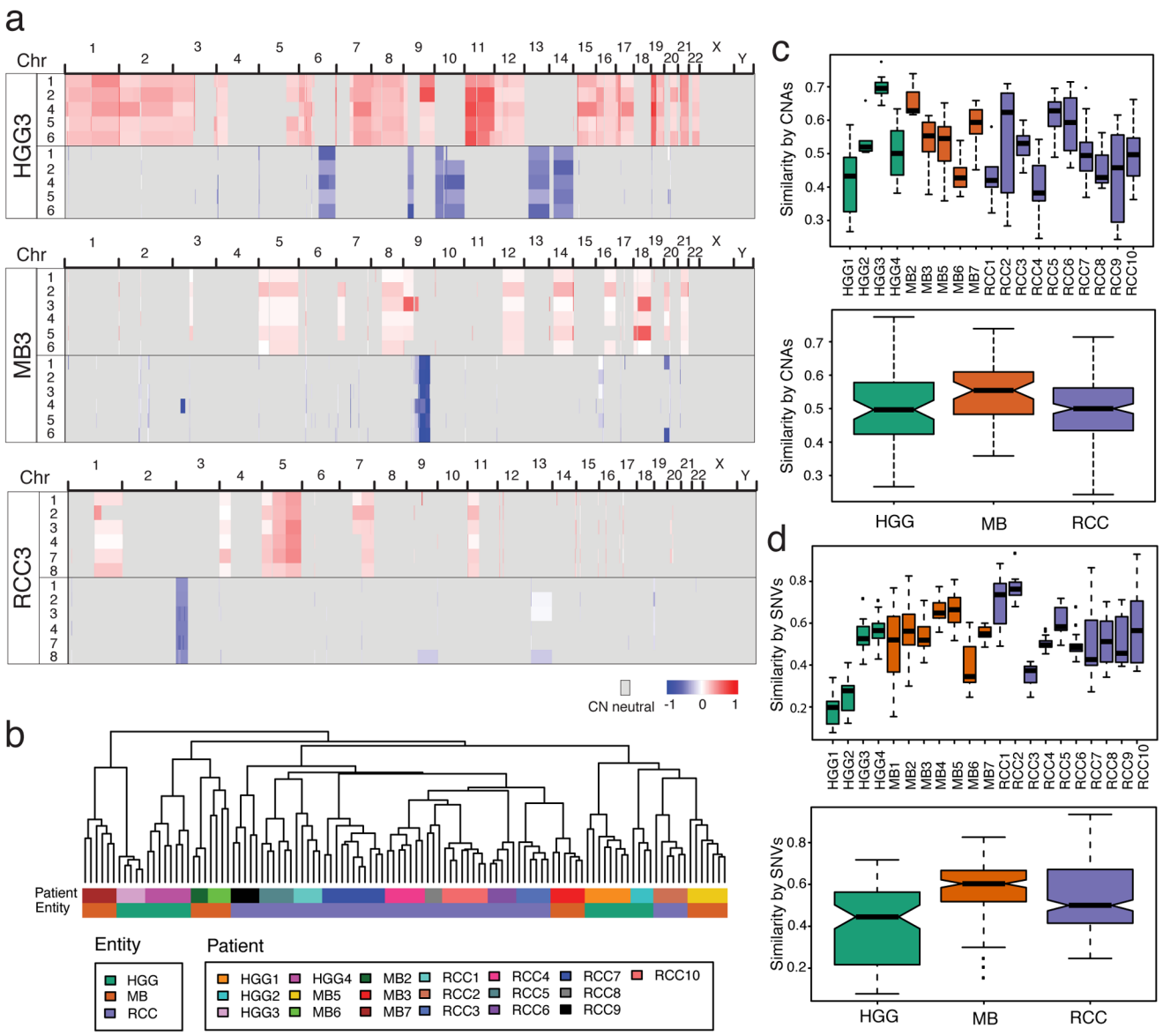

Figure 2. Variable intra-tumoral heterogeneity of somatic aberrations in all tumor entities

Genome wide analysis of copy number aberrations does not recapitulate the striking expression-based spatial homogeneity of MBs. **(a)** Copy number segments of gain (red) or loss (blue) are shown across the genome of three individual patients for each biopsy. **(b)** Unsupervised HCL of copy number segments show tight clustering of individual biopsies across all tumors in the cohort. Intra-tumoral heterogeneity measured from CNA's **(c)** or SNVs **(d),** both in individual patients (top panels) and summarized by entity (lower panels) shows that tumors in all entities range from high spatial similarity (e.g. HGG3, MB2) to low (e.g. HGG1, RCC3). Similarity is measured as the binary distance between all pairs of tumor-matched biopsies.

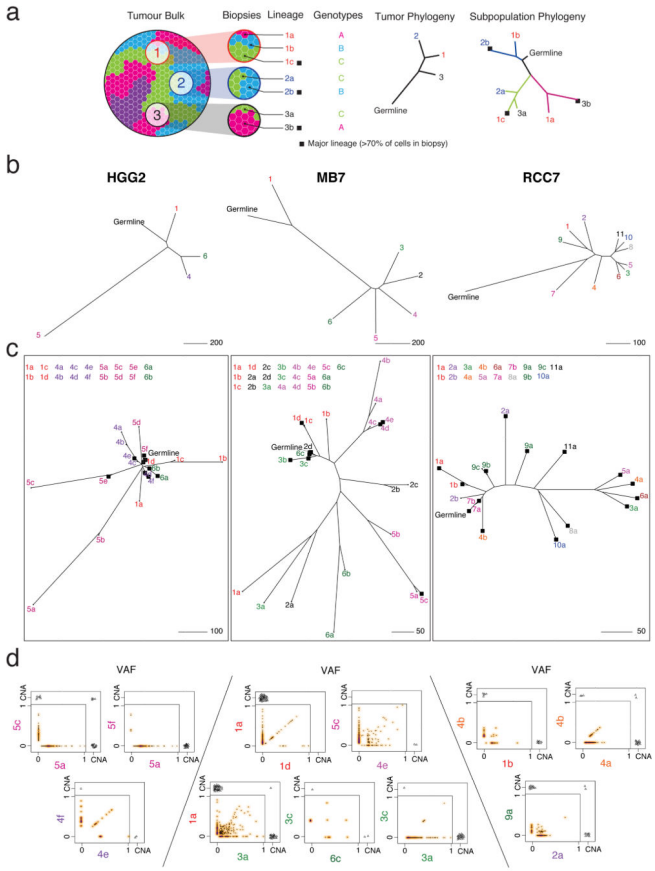

Figure 3. Spatial intermixing of clonal lineages

(a) Example cartoon of a tumor with four clonal lineages that are spatially dispersed (blue, green, pink, purple) demonstrates how data from three biopsies are used to build a typical biopsy-level phylogenetic tree as well as a subpopulation-level tree reflecting inter-mixing of the three detected genetic lineages. Branch tips are colored according to biopsy number and labeled according to biopsy number (1,2,3…) and clonal lineage (a,b,c…). Branch colors correspond to the cellular genotype; black squares indicate major cellular lineages (>70% of tumor cells in the biopsy, scaled by the largest detectable population). Note that the number of biopsies may not be sufficient to 'discover' all distinct clonal lineages (e.g. purple clone). **(b)** Biopsy-level trees of three representative tumors; MB7, HGG2, and RCC7. **(c)** Subpopulation-level trees reveal that some cellular lineages have high similarity to lineages in other biopsies, suggesting spatial intermixing (e.g. MB7 biopsy 1,2,3; RCC7 biopsy 4). Conversely, some biopsies harbor >1 distinct lineage (e.g. HGG2 biopsy 5)**. (d)** Variant allele frequency (VAF) of mutations are shown along with copy number aberrations exclusive to or shared by pairs of biopsies or subpopulations. VAF scatter plots have a smoothed color density; black dots represent individual mutations. CNA events (black triangles) are displayed (with some jitter) if present in either compartment, or shared.

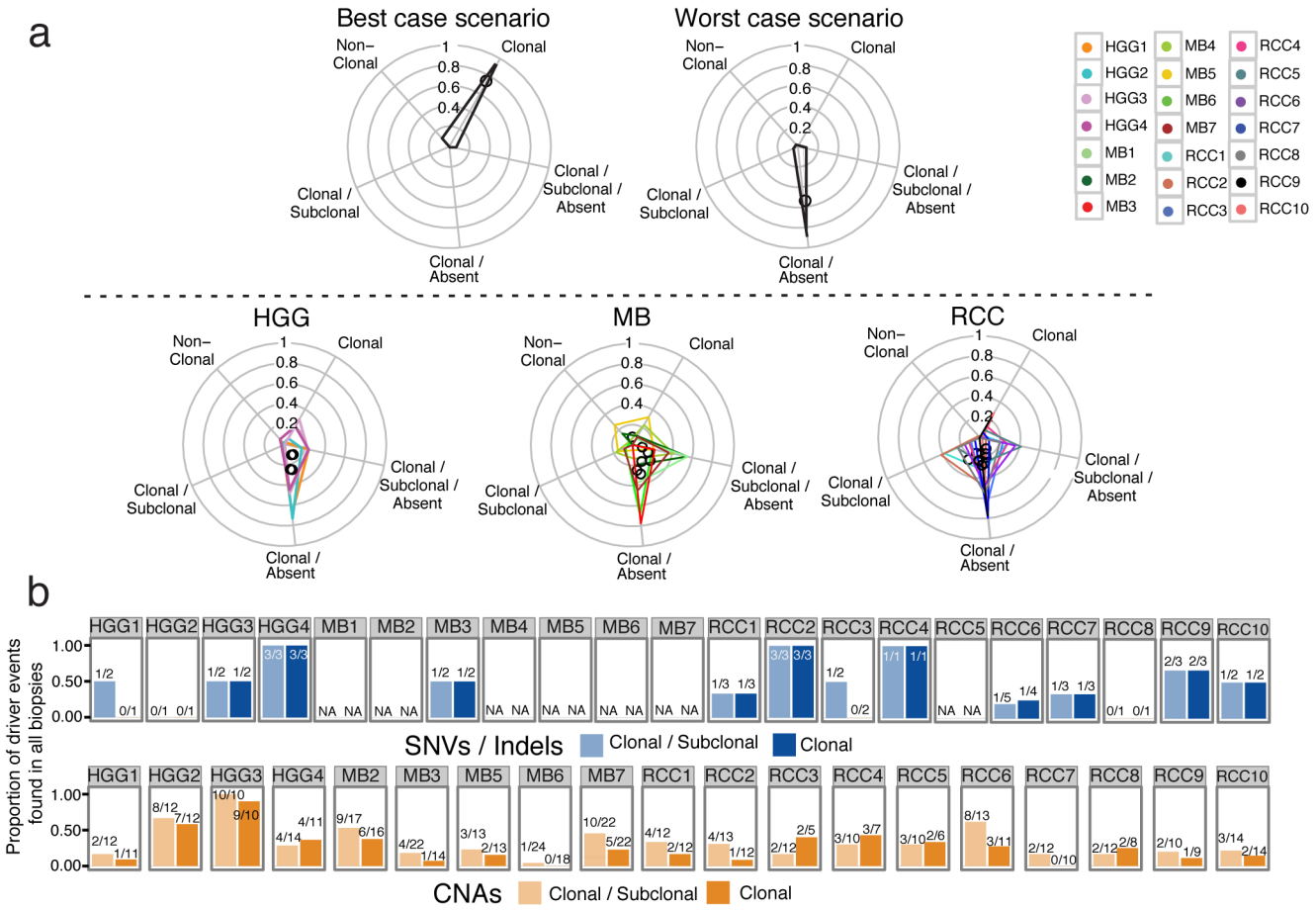

Figure 4. Genetically distinct clonal lineages yield ON/OFF mutation patterns between spatially separated biopsies

(a) Non-synonymous mutations are binned into 5 categories: those clonal in all biopsies (Clonal); clonal in some biopsies and sub-clonal in others (Clonal/Subclonal); clonal in some biopsies and completely absent in others (Clonal/Absent); clonal in some biopsies, sub-clonal in others, and absent in others (Clonal/Subclonal/Absent); and those never detected as clonal (Non-Clonal). *Upper panel*: illustration of the most favorable clinical scenario in which most mutations are clonal across all biopsies (left), and the worst-case scenario where mutations are clonal in some biopsies but absent in others (right). *Lower panel*: Mutation patterns follow a worst-case scenario across tumor types. Tumor-specific polygons on radial plots indicate the proportion of mutations on each of the 5 axes, with polygon centers marked by a black circle. **(b)** Barplots of the proportion of driver mutations/ indels (top panel) or CNAs (lower panel) that are found in every biopsy of a given tumor (i.e. trunk events) when considering the clonal and subclonal or only clonal driver events. The absolute numbers are shown above the bars.

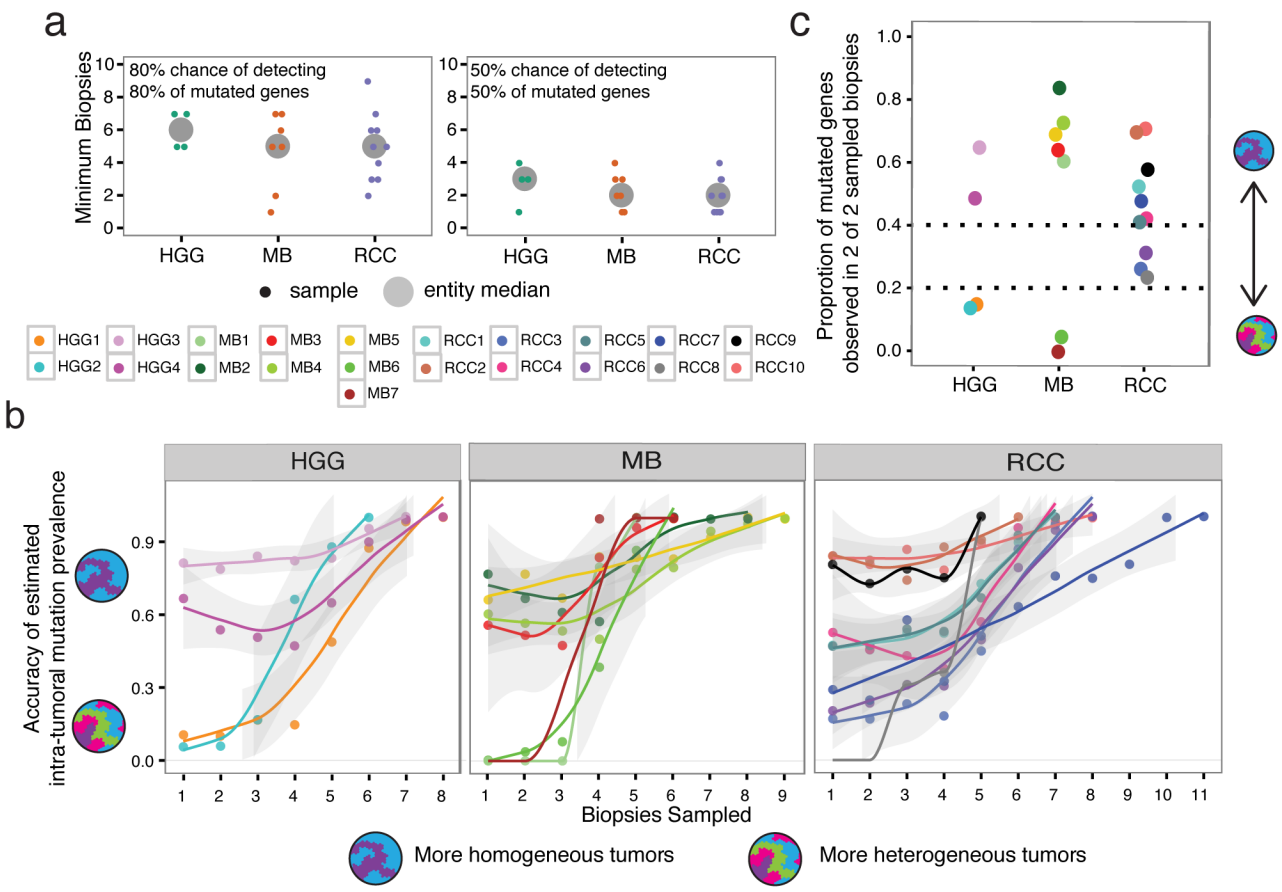

Figure 5. Quantification of variable genetic heterogeneity across tumor entities

(a) Considering all mutated genes (from the list of actionable targets) identified in each tumor across all biopsies, individual tumors require an average of 5 biopsies to have an 80% likelihood of recovering 80% of the known mutated genes (top panel). At least 2 biopsies are required to achieve a 50% likelihood of recovering 50% of mutated genes (bottom panel). Small points: individual samples; large points: tumor entity median. **(b)** The likelihood of correctly inferring the frequency of a mutation in the whole tumor depends on the number of biopsies sampled, and whether the tumor is more or less genetically homogeneous. The accuracy of frequency prediction for brain tumors shows a bi-modal pattern, with low genetic variance tumors having a higher accuracy (>0.6) even with few biopsies, while high genetic variance tumors require at least 5 biopsies to achieve the same confidence (HGG and MB panels). RCC tumors additionally show an intermediate pattern. Accuracy is measured as the proportion of times that a gene's observed frequency in a selection of biopsies is within 10% of the known frequency across all biopsies. Lines represent a Loess fit to the points per tumor, with a 95% confidence interval (grey outline). **(c)** Considering a random selection of 2 biopsies, patients are ranked using the proportion of mutated genes (from the actionable target list) that are present in both biopsies. Patients with genetically heterogeneous tumors have median values <0.2. Points represent the median value of all possible biopsy pairs per patient.

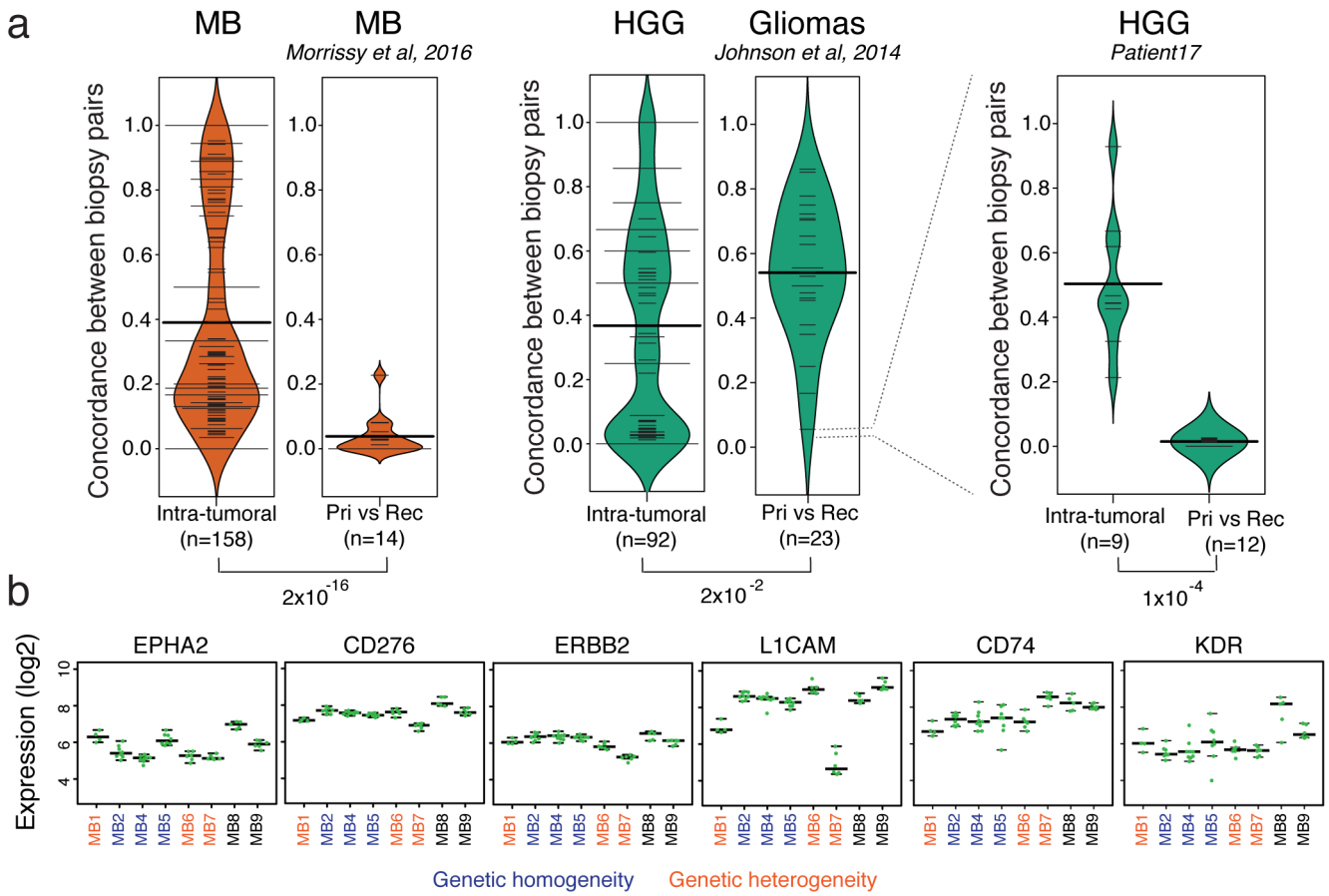

Figure 6. Genetic heterogeneity at recurrence greatly exceeds spatial heterogeneity in MB

(a) The genetic concordance of pre- *vs* post-therapy biopsies (from Morrissy *et al,* 2016) is an order of magnitude lower than up-front genetic spatial heterogeneity, in MB samples ($p<10^{-16}$; Welch two sample t-test; n=14 primary-recurrence pairs; n=158 spatial comparisons from 7 tumors). HGG tumors in our cohort showed a similar overall distribution of spatial heterogeneity (n=92 comparisons from 4 tumors), and not dramatically different compared to the low concordance of low-grade gliomas (LGG) to HGG post-therapy[41] (n=23 glioma primary-relapse pairs, Johnson *et al,* 2014). One LGG relapse to HGG exhibited post-therapeutic genetic concordance values on par with MBs ($p<10^{-4}$; Welch two sample t-test; n=12 primary-relapse comparisons from Patient17[32]; n=9 spatial comparisons). Concordance is measured as the proportion of clonal somatic mutations in common between a pair of biopsies given the total number of clonal somatic mutations in the two samples. Width of bean plots scale with the number of measurements with a similar y-value, showing data distribution. Thin horizontal lines indicate individual observations; multiple observations with the same value are added together to form wider lines; thick horizontal black bars indicate averages. **(b)** Low expression variance is observed across multi-region biopsies of cell surface molecules with immunotherapies currently in clinical trials. This indicates that tumors with high genetic spatial heterogeneity may respond well to CAR T-cell or antibody-based therapy. Green points mark expression of target genes

in individual biopsies; long horizontal lines: median expression per tumor; lower and upper short horizontal lines: 25^{th} and 75^{th} percentiles of expression per tumor.